Journal of Renewable Materials

Tech Science Press

DOI: 10.32604/jrm.2022.021473

check for updates

ARTICLE

Fully Bio-Based Composites of Poly (Lactic Acid) Reinforced with Cellulose-Graft-Poly-(ε-Caprolactone) Copolymers

Chengtao Gao[1,2], Yang Wu[3] and Haibo Xie[1,*]

[1]College of Materials and Metallurgy, Guizhou University, Guiyang, China

[2]National Engineering Research Center for Compounding and Modification of Polymer Materials (Guizhou Material Industrial Technology Institute), Guiyang, China

[3]College of Materials Science & Engineering, University of Nanchang, Nanchang, China

[*]Corresponding Author: Haibo Xie. Email: hbxie@gzu.edu.cn

Received: 16 January 2022 Accepted: 23 May 2022

ABSTRACT

Due to the increasing demand for modified polylactide (PLA) meeting "double green" criteria , the research on sustainable plasticizers for PLA has attracted broad attentions. This study reported an open-ring polymerization method to fabricate cellulose (MCC)-g-PCL (poly (ε-caprolactone)) copolymers with a fully sustainable and biodegradable component. MCC-g-PCL copolymers were synthesized, characterized, and used as green plasticizers for the PLA toughening. The results indicated that the MCC-g-PCL derivatives play an important role in the compatibility, crystallization, and toughening of the PLA/MCC-g-PCL composites. The mechanical properties of the fully bio-based PLA/MCC-g-PCL composites were optimized by adding 15 wt% MCC-g-PCL, that is, the elongation at break was 22.6% (~376% higher than that of neat PLA), the tensile strength was 47.3 MPa (comparable to that of neat PLA), and the impact strength was 26 J/m (~130% higher than that of neat PLA). DSC results indicated that MCC-g-PCL reduced the T_g of the PLA blend. When the addition amount was 15 wt%, the T_g of the blend was 58.4°C. Compared with MCC, MCC-g-PCL polyester plasticizer has better thermal stability, $T_{5\%}$ (°C) can still be maintained above 300°C. The rheological results showed that MCC-g-PCL acted as a plasticizer, the introduction of PCL flexible chain increased the mobility of PLA molecular chain, and decreased the complex viscosity, storage modulus and loss modulus of PLA blends. The MCC-g-PCL derivatives , as a new green plastic additive, have shown an interesting prospect to prepare fully bio-based composites.

KEYWORDS

Green plasticizers; PLA; cellulose (MCC)-g-PCL; fully bio-based composites

1 Introduction

The growing consumption of crude oil on human development highlights the concern of the resource availability and environmental crisis. On this account, the renewable and sustainable polymeric materials have become a mainstream research topic [1–3]. The transformation of the traditional petro-based plastics to bio-based polymeric materials not only brings a new blueprint for resource richness, but also provides benefits to our environment [4–7]. The sustainable poly (lactide) (PLA) is a bio-based thermoplastic polyester, which is polycondensated from lactic acid, and has a variety of carbohydrate sources, including

corn, sugarcane or tapioca. It can supply the sugar source to obtain lactic acid by fermentation [8,9]. In general, PLA has been intensely researched due to its precursor (lactic acid) from renewable biomass, providing a "befitting" alternative to fossil-based materials. Moreover, the attracting traits of biodegradation and biocompatibility endows these polymers can be hydrolyzed to lactic acid and metabolized to water and carbon dioxide [4,10]. However, as other synthetic plastics, PLA has its inherent drawback such as inherent brittleness, poor impact and tear resistance, and slow recrystallization rate, which limit its applications in biomedical, automotive, and structural fields. The focus of PLA modification is to produce renewable materials to make up for the shortcomings of PLA [11–13].

Recently, a new definition of "double green" has been prevalent in composites process, which includes ideal plasticizer and sustainable polymer matrix [14,15]. The green plasticizer should be the renewable resources and easy to biodegrade in the landfill, and have excellent machinability and satisfactory chemical stability under processing conditions, and low price and high availability. PLA is a befitting polymer matrix candidate to meet the "double green" criteria. It has become a central issue to use green plasticizers to toughen its crystal morphology without losing the mechanic properties of PLA [14,16,17].

Natural polymers have gained significant attention due to their natural renewable, low-cost, biodegradable, and eco-friendly properties [18,19]. Cellulose, is an important natural biopolymer and the main biomass. It has unique properties, including renewability, high thermal stability and biodegradability [20,21], however, the lack of solubility in common organic solvents limits its utilization in homogenous modifications. Thus, the dissolution of cellulose is the key step for their application. As one of the main the greenhouse gas, the carbon dioxide (CO_2) has an undesirable impact on ecological environment. However, CO_2 can be used as a main C1 resource through capture and storage [22,23]. Recently, a more sustainable CO_2-based solvent system for dissolution of cellulose has been presented by Xie et al. almost simultaneously [24,25]. The novel dissolving systems will bring a promising grafting strategy to obtain the new cellulosic materials, which can improve the processability and endow new functionality of cellulose. Graft polymerization is one of the most promising and effective ways to change the physical and chemical properties of cellulose. It can extend application of cellulose by incorporating different polymer components at the molecular structure level [26]. Lönnberg et al. [27] have synthesized cellulose-g-PLA/PCL derivatives based on cotton pulp cellulose, and modified cellulose with 2,2-bis (methyl) propionic acid to introduce more available hydroxyl groups on the surface, the results showed that the grafting efficiency of cellulose was significantly improved after modification. Xu et al. [28,29] have prepared serials of cellulose-g-PCL copolymers via *in situ* ROP by ε-caprolactone, the poly(ε-caprolactone) (PCL) got much due to their excellent biodegradability, biocompatibility, low immunogenicity, nontoxicity, which has promising application in implantable biomedical materials and sustainable bio-nanocomposites. Introducing polymer segments with similar structure and polarity to the surface of cellulose is an effective way to improve the compatibility between cellulose and polymer matrix, which can better control the comprehensive properties of polymer composites.

Microcrystalline cellulose (MCC) are rodlike defect free crystalline nanoparticles obtained after the acid hydrolysis of cellulose fibers. Recently, CNW has attracted great attention not only because of its abundance, renewability and sustainability, but also because of their excellent physical and chemical properties. They have been widely studied as reinforcing agents in nanocomposites because of their low cost, availability, renewability, lightweight, nanoscale dimension, and unique morphology. Sheng et al. [30] have prepared poly (lactic acid) (PLA)/bamboo cellulose nanowhiskers (BCNW) composite which was reinforced by silane surface-modified ultrafine bamboo-char (UFBC) with a high toughness but a low modulus, the results showed that BCNW and UFBC produced a synergistic effect on composites' toughening and strengthening. The novel nanofibrillated celluloses (NFCs) were used to reinforce non-plasticized and green-plasticized PLA composites. The addition of NFCs not only enhanced the strength and toughness remarkably, but it also improved the thermal stability of PLA composites, which has been presented by

Xu et al. [31]. Cellulose used to reinforce PLA has been reported in the literature. However, the cellulose and its derivatives were not investigated as PLA plasticizers so far.

In this work, the sustainable MCC-g-PCL copolymers are fabricated by open-ring polymerization (ROP) with ε-caprolactone in an efficient cellulose dissolution system. The structure of the copolymers is investigated by Fourier transform infrared spectroscopy (FTIR) and NMR spectra. The MCC-g-PCL copolymers as green plasticizers are added into the PLA/MCC-g-PCL composites as green plasticizers by twin-screw extrusion. MCC-g-PCL derivatives play an important role in the compatibility, crystallization, and toughening of the PLA/MCC-g-PCL composites. The compatibility effects of MCC-g-PCL with PLA matrix on the mechanical properties and thermal performances of the composites are analyzed and discussed by mechanical tests, DSC and TGA. Consequently, this study is expected to provide a comprehensive understanding of the behaviors of the MCC-g-PCL during the processing of PLA modification.

2 Experimental

2.1 Materials

Microcrystalline cellulose (MCC, DP = 220, particle size: ~50 μm), 1,8-diazabicyclo [5.4.0] undec-7-ene (DBU) and MCC were purchased from Aladdin Reagents Co., Ltd. (Shanghai, China). Analytical grade Methyl alcohol and dimethyl sulfoxide (DMSO) were purchased from Kermel Reagents Co., Ltd. (Tianjin, China). DMSO was dried using 4 A molecular sieves prior to the experiments. CO_2 was purchased from Guiyang Shenjian Gas Co., Ltd. (Guizhou, China) with a purity of >99.99%. The ε-caprolactone (ε-CL, purity: 99%) were obtained from Aladdin Commerce Reagent Co., Ltd. (China) and was dried over CaH_2, and distilled under reduced pressure before use. The DBU was dried by KOH, and then purified by distillation. Polylactide (PLA 4032D) with a weight-average molecular weight (M_w) and a polydispersity index of 1.76×10^5 g/mol and 2.1 was provided by Natureworks, USA. All other chemicals were of analytical grade and use without further purification.

2.2 Preparation of MCC-g-PCL Copolymers

Microcrystalline cellulose (MCC) (5%) was suspended in the mixed solution 1,8-diazabicyclo [5.4.0] undec-7-ene (DBU) and DMSO in a stainless reactor, the reactor with 0.5 MPa of CO_2 pressure was shifted in a 50°C Oil bath after the replacement of the air by CO_2 for three times. Achieving a clean cellulose solution, ε-CL (2.64 g, 23.1 mmol) was dropped into a flask equipped with a mechanical stirring under N_2 atmosphere at 80°C that contained 5 g of 5 wt% of the prepared cellulose solution. The ring opening graft polymerization was conducted at 110°C for 24 h. After being cooled down to room temperature, the prepared copolymer was precipitated with methanol and washed several times to remove the unreacted monomer, DBU and DMSO. Subsequently, the copolymer was suspended in dichloromethane and magnetically stirred at room temperature for 48 h to remove the homo-PCL. The purified copolymer was vacuum-dried at 50°C for 24 h.

2.3 Preparation of Composites

Both the MCC-g-PCL and PLA were dried in vacuum for 12 h at 80°C before well mixture according to a contrivable mass fraction. A series of PLA/MCC-g-PCL blends were prepared and abbreviated as PLA/*x*-MCC-g-PCL, *x* represents the contents of MCC-g-PCL varying from 5 wt% to 10 wt%, 15 wt% and 20 wt%. For the preparation of the composites, the above mixed material was extruded on a SJZA-10A micro-twin screw extruder (Wuhan Ruiming Experimental Instrument Co., Ltd., Wuhan, China). The screw speed of the main engine is 50 r/min, the feeding speed is 30 r/min, and the temperature of each heating section is 180°C, 185°C and 195°C, respectively. And then, the extruded samples were formed by the SZS-20 microinjection machine (Wuhan Ruiming Experimental Instrument Co., Ltd., Wuhan, China) to obtain

the stretch and impact splines (the cylinder temperature and mold temperature are 210°C and 60°C, respectively). After injection, the samples were placed in a constant temperature biochemical chamber (temperature 23°C, humidity 80%) for 24 h to eliminate internal stress and for further analysis.

2.4 Characterization and Measurements

2.4.1 Fourier-Transform Infrared (FTIR) Spectroscopy

The FTIR spectra of neat PLA, MCC-g-PCL, PLA/20%MCC and PLA/MCC-g-PCL blends were recorded on a Bruker Tensor 27 spectrometer. Spectra were recorded over the range of 4000 to 400 cm^{-1} with the resolution and scanning number of 4 cm^{-1} and 32 time, respectively. All samples for FTIR analysis were prepared by pressing with KBr.

2.4.2 Nuclear Magnetic Resonance (NMR) Spectroscopy

The ^{1}H-NMR and ^{13}C NMR spectra of MCC-g-PCL were recorded on a Bruker Ascend 400 spectrometer (Bruker Corporation, Karlsruhe, Germany) with specimens in DMSO-d_6 at room temperature, Usually, 100 scans and 10000 scans for the ^{1}H-NMR and ^{13}C NMR spectra, respectively. Chemical shifts (δ) are reported in parts per million (ppm) with the residual solvent peak of tetramethylsilane used as the internal standard at 0.00 ppm.

2.4.3 Scanning Electron Microscopy (SEM)

The cryogenically fractured morphologies of the PLA/MCC-g-PCL composites were taken by using a Quanta FEG250 scanning electron microscopy (SEM) (FEI Co., Ltd., Hillsboro, OR, USA) instrument with an acceleration voltage of 25 kV. SEM images were recorded after the surfaces of the samples were coated with gold.

2.4.4 Differential Scanning Calorimetry (DSC)

The DSC curves of neat PLA, MCC-g-PCL and PLA/MCC-g-PCL blends were recorded on a Q50 thermal gravimetric analyzer (TA Instruments, Co., Ltd., New Castle, Pennsylvania, USA). All the measurements were conducted under a nitrogen atmosphere. The samples with ∼10 mg were first melted at 200°C for 5 min to remove thermal history, and then quenched to −90°C at a rate of 10°C/min, and finally reheated to 200°C at a rate of 10 °C/min after maintaining at −90°C for 5 min. The last heating curve was recorded for analysis. Relative crystallinity is calculated by the formula $\mathrm{Xc}(\%) = \dfrac{\Delta \mathrm{Hm} - \Delta \mathrm{Hcc}}{\chi.\Delta \mathrm{H0}} \times 100\%$, where χ is the weight content of PLA in the PLA/MCC-g-PCL composites. ΔH_m is the melting enthalpy of PLA/MCC-g-PCL composites. ΔH_o is on behalf of the melting enthalpy of 100% crystalline PLA, which is 94 $J{\cdot}g^{-1}$ [32]. ΔH_{cc} represents cold crystallization enthalpy.

2.4.5 Thermogravimetric Analysis (TGA)

TGA curves of neat PLA, MCC-g-PCL and PLA/MCC-g-PCL blends were performed on a Q50 thermal gravimetric analyzer (TA Instruments, Co., Ltd., New Castle, Pennsylvania, USA). The measurements were carried out under 60 mL min^{-1} N_2 gas flows using ceramic crucibles containing 10 mg of sample. All samples were heated to 600°C using a heating rate of 10 °C/min.

2.4.6 Mechanical Properites

The tensile strength of the samples with dimensions of 75 mm (length) × 5 mm (width) × 2 mm (thickness) were examined on a universal testing machine (CMT6104, Shenzhen SANS test machine, China) and the test mode under a stand (ISO 527). The strain rate at 5 mm/min, the gauge length between the two pneumatic clamps was 25 mm. The measurements were conducted at 25°C and a relative humidity of 50% ± 5%, five replicate specimens were tested, and the average values were reported. The spline in QYJ1251 notch specimen, gap depth is 2.0 mm, cracking tip curvature radius is 0.25 mm, the processed notch specimen was kept at room temperature for 24 h, and the notch Izod

impact strength was determined by a ZBC-4B type plastic pendulum impact testing machine (Shenzhen New Think Measurement Technology Co., Ltd., China), using the ISO 180 standard. Each sample was measured at least five times, and the results were reported on average.

2.4.7 Rheological Behavior

Rheological behavior was performed on a Haake Mars60 (Thermo Scientific Instruments) rotational rheometer with a parallel plate geometry (diameter: 25 mm) and a gap of 1 mm. Oscillatory frequency sweeps were performed from 0.01 Hz to 100 Hz at 180°C with a strain of 1%.

3 Results and Discussion

3.1 The Structure of MCC-g-PCL Copolymers

The structure of the grafted copolymer is confirmed by NMR spectra, as shown in Fig. 1. The peaks at δ = 4.65, 3.78, 3.57 and 3.05 ppm belong to the resonance of H_1, H_3, $H_{2,5,6}$ and H_4 in the AGU units of the cellulose, respectively. Meanwhile, the signals at δ = 5.51, 5.37 and 4.32 ppm correspond to the protons of the residual unreacted hydroxyl groups of AGU units. The new signals at δ = 4.0 and 3.37 ppm are attributed to the internal $–CH_2O–$ repeating units (H_e) and $–CH_2OH$ end units ($H_{e'}$), respectively. The peaks at δ = 1.53 and 2.26 ppm are assigned to the internal $–COCH_2–$ repeating units (H_a) and terminal $–COCH_2–$ ($H_{a'}$), respectively. The signals at δ = 1.40 and 1.30 ppm should be attributed to the methylene hydrogen ($–CH_2–$, H_b and H_d) and the H_c, respectively. The signal at 173.1 ppm is assigned to the carbonyl carbons of the PCL side chains. The peaks at chemical shifts of 102.0, 70.0, 76.9, 80.6 and 63.5 ppm are ascribed to the C_1, $C_{2,3,5}$, C_4 and C_6 carbons on the AGU units, respectively. In addition, a peak around 60.3 ppm is assigned to the $C_{6'}$ carbon bearing a substitute PCL side chain. Moreover, the peaks at δ = 32.0, 33.7, 25.1, 24.1, 27.7, 60.3 and 63.5 ppm are attributed to the carbons in the a, a′, b, c, d, e and e′ positions, respectively. According to these chemical shifts and the corresponding integrals, the degree of polymerization of PCL (DP), the molar substitution of PCL (MS), the degree of substitution of PCL (DS, the grafted PCL side chains per cellulose repeating unit), and the weight content of PCL (W_{PCL}) were calculated by the following formulas [8]:

$$DP = \frac{I_a + I_{a'}}{I_{a'}} \tag{1}$$

$$MS = \frac{I_a + I_{a'}}{2H4} \tag{2}$$

$$DS = \frac{I_{a'}}{2H4} \tag{3}$$

$$W_{PCL} = \frac{MS \times 114}{162 + MS \times 114} \times 100\% \tag{4}$$

where I_{H4}, I_a and $I_{a'}$ are the corresponding integrals of H_4, H_a and $H_{a'}$ in Fig. 1A, the coefficients of 162 and 114 are the molecular weights of the AGU unit and ε-CL monomer. Table 1 shows those experimental conditions and these results of PCL on cellulose.

The incorporation of MCC-g-PCL and cellulose into the PLA matrix has been confirmed by FTIR, as shown in Fig. 2. In order to identify and compare the bands related to MCC-g-PCL and PLA, the cellulose is also displayed in the spectra. Characteristics bands of PLA bond vibrations are strong absorptions bands at 1750 cm^{-1}, ascribed to the stretching vibrations of –C=O, and at 1180 cm^{-1}, is related to the C–O–C stretching mode. Compared with MCC, a new band for MCC-g-PCL at 1715 cm^{-1}, which is attributed to the carbonyl group. After MCC-g-PCL adding into PLA matrix, the absorption band at 1725 cm^{-1} is

attributed to –C=O stretching vibration in the ester groups. With the increase of MCC-g-PCL in the composites, the intensity of –C=O stretching vibrations increases gradually.

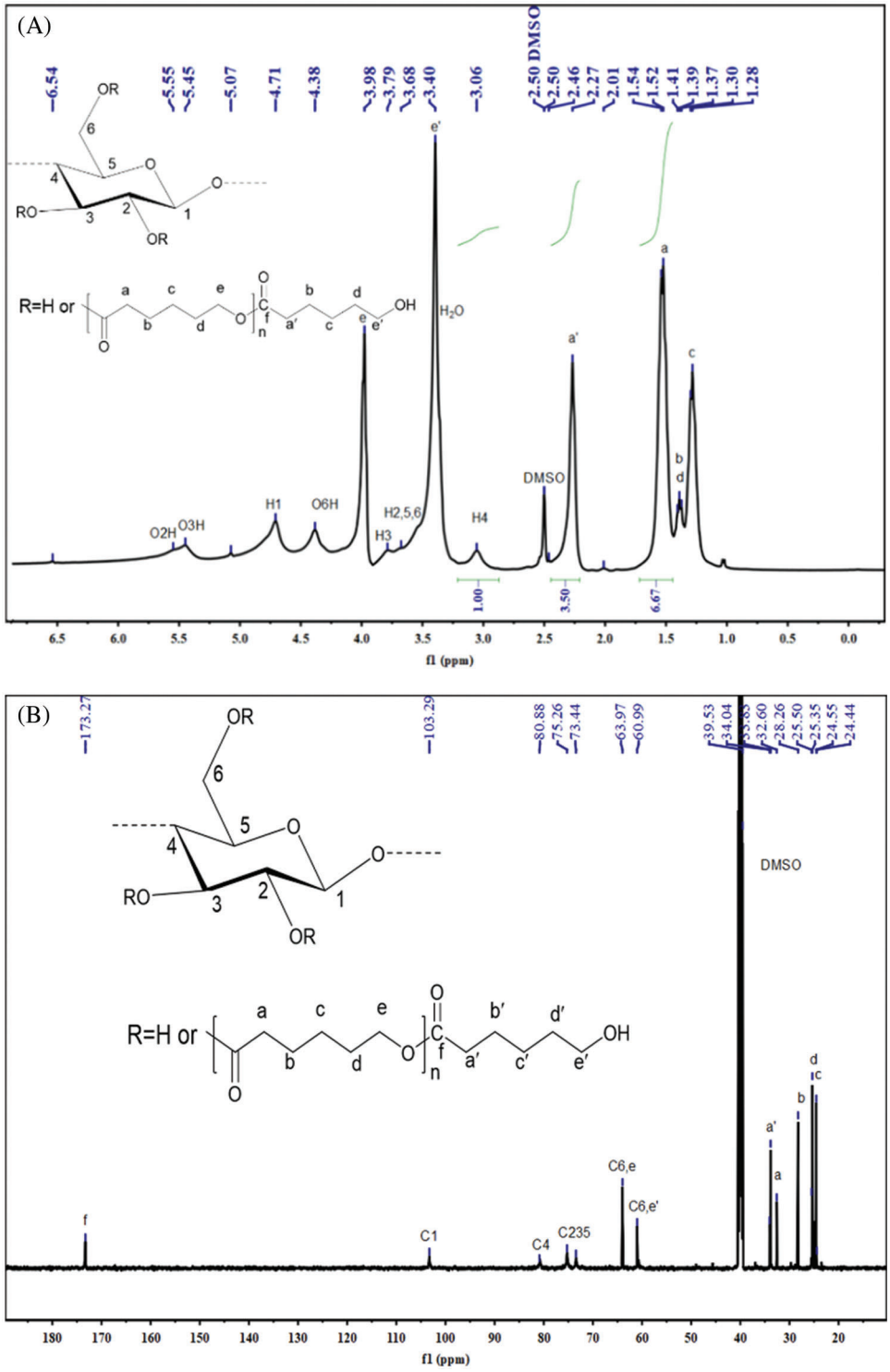

Figure 1: The ^{1}H NMR (A) and ^{13}C NMR (B) spectra of MCC-g-PCL (DS = 1.75)

Table 1: Experimental conditions[a] and results of MCC-g-PCL derivatives

Entry	CL/AGU (mol/mol)	T (°C)	Time (h)	DP_{PC}[b]	MS_{PCL}[b]	DS_{PCL}[b]	W_{PCL}[b] (%)	M_w (g/mol)
1	5	110	24	2.91	5.09	1.75	78.2	1.63×10^5

Note: [a] Experimental conditions: Cellulose concentration 5 wt%; The molar ratio of ε-CL to AGU in cellulose was 5/1; Reaction temperature and time were 110°C and 24 h, respectively.

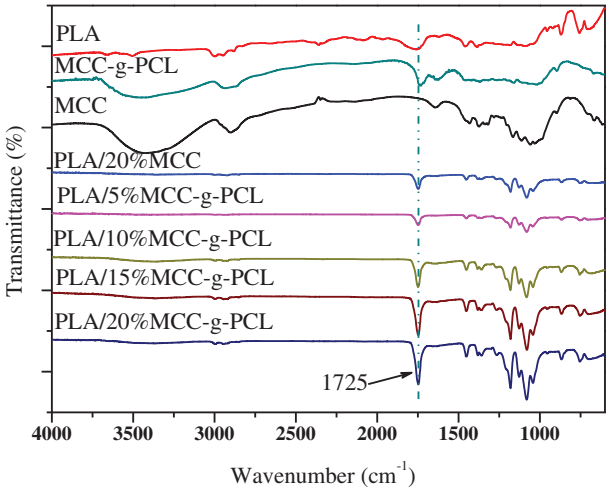

Figure 2: FTIR of neat PLA, PLA/20% MCC binary blends, cellulose-g-PCL and cellulose-g-PCL/PLA composites with different content of MCC-g-PCL

3.2 Morphology Analysis

The morphology characterization of the cross-sectional topography of neat PLA, PLA/20%MCC and PLA/MCC-g-PCL composites with different contents of MCC-g-PCL are shown in Fig. 3. The transition from brittle fracture (Figs. 3A and 3B), through elastic-plastic stable fracture followed by unstable crack propagation (Figs. 3C and 3D), to elastic-plastic fracture with stable crack propagation (Fig. 3E), and back to elastic-plastic fracture with unstable crack propagation (Fig. 3F) could be differentiated clearly on the fracture surfaces. It can be seen from Figs. 3A and 3B (red arrow) that neat PLA and PLA/20%MCC show a typical brittle fractured morphology with a very smooth and compact surface. In fact, the MCC and PLA without strong interfacial interactions. There are also many grooves and holes in the rough cross section (red arrow in Fig. 3B), which are from the cellulose unit formation due to the strong effects of hydrogen bonds, and the poor dispersion state of cellulose in the PLA matrix results in interfacial incompatibility. With the addition of MCC-g-PCL into PLA, the fracture surface of the PLA/MCC-g-PCL composites becomes more irregular due to the plastic deformation. It is also observed that MCC-g-PCL is more uniformly dispersed in PLA, as shown in Figs. 3C–3F. It is interesting to find that a large number of rough, uneven wrinkles and uniform cavities appear in the surface of PLA/5%MCC-g-PCL, PLA/10% MCC-g-PCL and PLA/20%MCC (red arrow). This indicates that the composites undergo internal cavitation during the cryo-fracture process [17]. When the material is stretched by external force, the relative slippage of the PLA molecular chains and particles can cause relative motion. PLA/15%MCC-g-PCL (Fig. 3E) exhibit uniform fractured surfaces, indicating that the MCC-g-PCL has a well-distributed state in the composites. From the above discussion, it is concluded that the introduction of MCC-g-PCL polyester improves the compatibility between cellulose and the PLA phase due to the green MCC-g-PCL plasticizer uniformly dispersed in PLA.

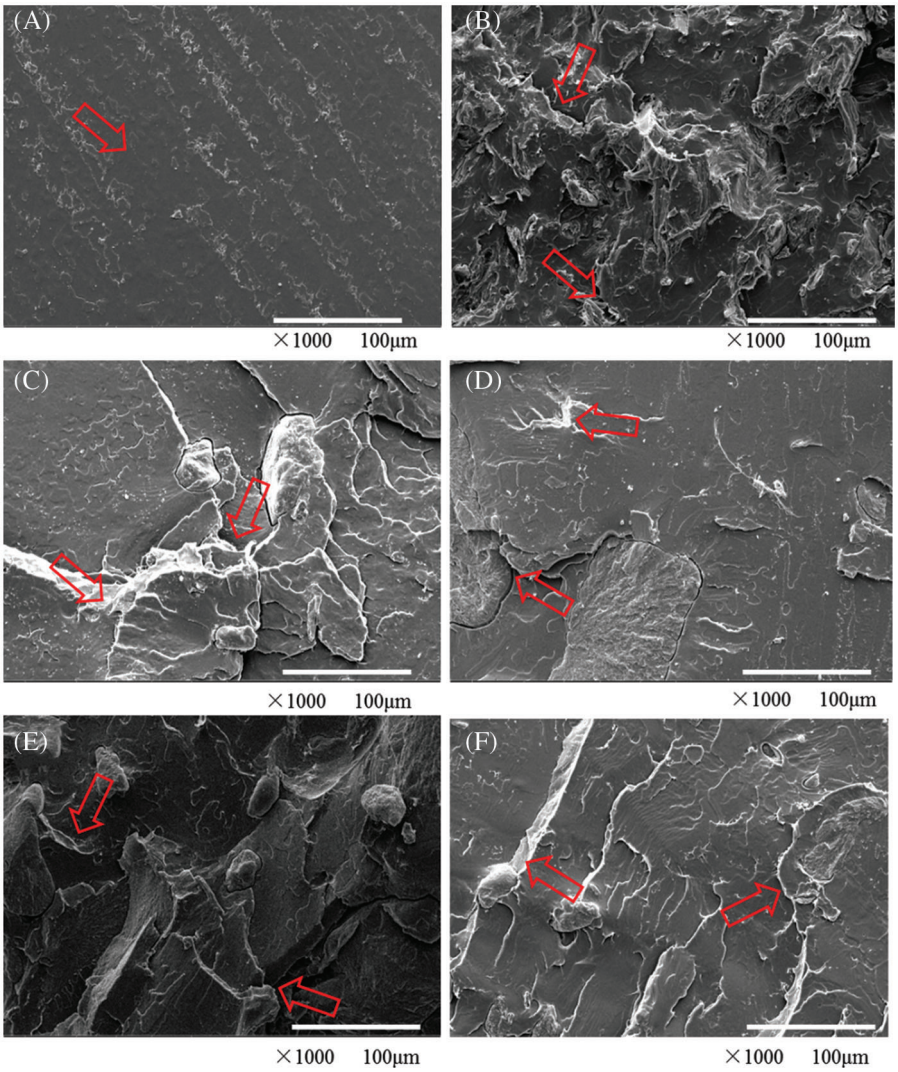

Figure 3: SEM images of fracture surfaces for (A) PLA; (B) PLA/20%MCC; (C) PLA/5%MCC-g-PCL; (D) PLA/10%MCC-g-PCL; (E) PLA/15%MCC-g-PCL; (F) PLA/20%MCC-g-PCL

3.3 Thermal Properties

The TGA and DTG curves of PLA, PLA/MCC and PLA/MCC-g-PCL composites are shown in Figs. 4 and 5, respectively. The corresponding TGA data are listed in Table 2. The thermal decomposition temperature of MCC, PLA/20%MCC and neat PLA are 330.0°C, 347.3°C, and 357.5°C, respectively. The results indicate that the thermal decomposition temperature of the composites is close to neat PLA. The thermal decomposition temperature of PLA/20%MCC decrease by about 10°C compared with neat PLA. This is attributed to that neat cellulose fiber maintains a lower thermal decomposition temperature. Fig. 6 also shows that the maximum decomposition rate of pristine PLA is higher than that of PLA/20% MCC and PLA/MCC-g-PCL composites, meanwhile the temperature at maximum decomposition rate of PLA/MCC-g-PCL composites shifts to a lower temperature, which proves that the addition of MCC-g-PCL slightly accelerates the thermal degradation of composites.

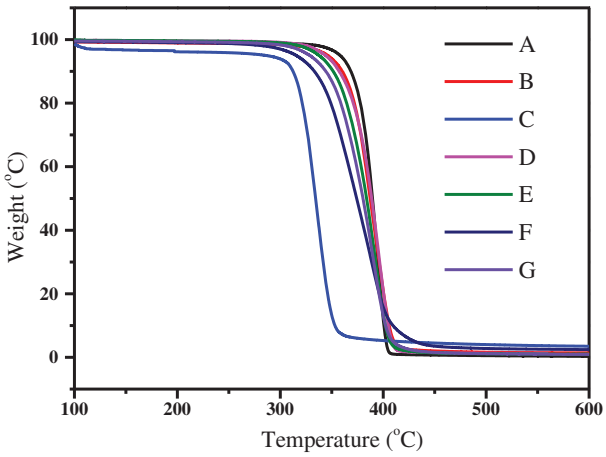

Figure 4: TGA curves for neat PLA and its composites with different content of MCC-g-PCL in the N_2 atmosphere: (A) PLA; (B) PLA/20%MCC; (C) MCC; (D) PLA/5%MCC-g-PCL; (E) PLA/10%MCC-g-PCL; (F) PLA/15%MCC-g-PCL; (G) PLA/20%MCC-g-PCL

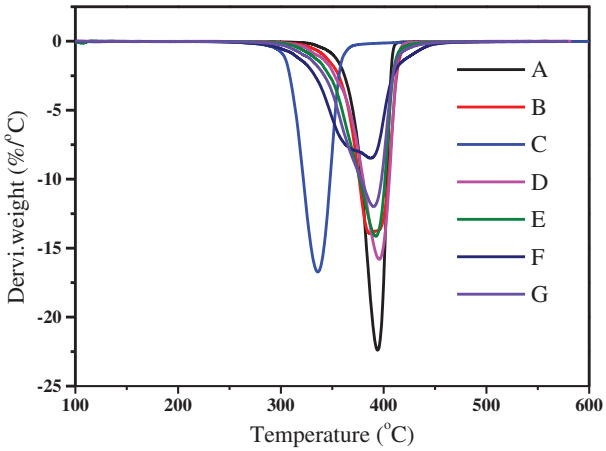

Figure 5: DTG curves for neat PLA and its composites with different content of MCC-g-PCL in the N_2 atmosphere: (A) PLA; (B) PLA/20%MCC; (C) MCC; (D) PLA/5%MCC-g-PCL; (E) PLA/10%MCC-g-PCL; (F) PLA/15%MCC-g-PCL; (G) PLA/20%MCC-g-PCL

Table 2: Thermal properties of neat PLA and its composites

Samples	$T_{5\%}$ (°C)	T_{onset} (°C)	T_{max} (°C)
PLA	358.0	377.0	402.7
MCC	285.0	319.2	350.8
PLA/20%MCC	346.1	367.4	408.1
PLA/5%-MCC-g-PCL	343.9	370.6	407.4
PLA/10%-MCC-g-PCL	337.6	363.3	404.8
PLA/15%-MCC-g-PCL	315.4	340.5	408.0
PLA/20%-MCC-g-PCL	328.6	356.3	405.2

Note: T_{onset}: Temperature of initial decomposition; $T_{5\%}$: Temperature of decomposition at 5%; T_{max}: Temperature of maximum decomposition.

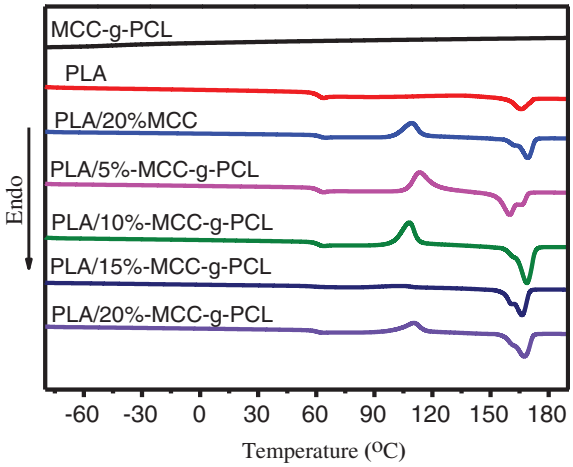

Figure 6: DSC curves for neat PLA and its composites in the N_2 atmosphere

The DSC curves of the samples from −90°C to 200°C are recorded to investigate the non-isothermal crystallization and melting behavior of neat PLA, PLA/20%MCC and PLA/MCC-g-PCL composites in the N_2 atmosphere, as shown in Fig. 6, and the corresponding DSC data are exhibited in Table 3. Glass transition temperature (T_g) is usually used to describe the miscibility between the polymer matrix and the additive [33]. The results show a low T_g value of −43.9°C with DS_{PCL} value of 1.75, which is attributed to the grafting polymerization of PCL onto cellulose as a plasticizer in an expansion of intermolecular distance and an enhancement of the PLA chain mobility. The T_g value of neat PLA is 63.3°C, and the PLA/MCC-g-PCL composites have a slightly lower average T_g of 60.4°C. The T_g values of PLA composites decrease slightly in lower temperature range with increasing the content of MCC-g-PCL, which is ascribed to the increase of chain mobility of PLA due to the presence of MCC-g-PCL derivatives. The DSC data indicates that MCC-g-PCL can significantly promote the crystallization of PLA (Table 4). The cold crystallization temperature of neat PLA is 133.5°C with a gentle crystallization peak and a low crystallinity of 3.9%, indicating that neat PLA has a weak crystallization ability because the rigid PLA chain segments are difficult to arrange into ordered crystal phase. All the PLA/MCC-g-PCL composites with an average cold crystallization temperature of ~109°C and an average crystallinity ~16.3% shows obvious cold crystallization peaks, and the peak temperature shifts to lower temperature range with increasing the MCC-g-PCL content in comparison with neat PLA. The crystallinity of the samples increases initially and then decreases with the increasing the MCC-g-PCL content. Furthermore, when the MCC-g-PCL content is 15 wt%, the composites show the highest crystallinity of ~29.4%, indicating that the crystallization ability of PLA composites is significantly improved by the MCC-g-PCL derivatives. The crystallization induced by MCC-g-PCL may be the origin of this enhanced adhesion and homogeneous microstructure. This fact was clearly observed in the case of unmodified MCC particles with lower affinity to PLA. In the opposite, low molecular weight CL segment in the MCC-g-PCL has higher affinity to PLA, thus giving rise to a homogeneous blend according to SEM analyses. MCC-g-PCL is uniformly dispersed in the PLA matrix, as shown in Figs. 3C–3F. It acts as a good nucleating agent in the crystallization process of PLA and promotes heterogeneous nucleation of PLA. Therefore, the crystallizing ability of composites are obviously enhanced with the increasing the content of MCC-g-PCL. The DSC curve shows that the melting shoulder of PLA/MCC-g-PCL composites has a slightly lower than the melting peak, which is due to the imperfect crystalline region of the composites during melting process. The presence of such double melting peak in the case of PLA is a well-known phenomenon caused by the modification of the PLA crystal growth. This phenomenon is often ascribed to the coexistence of two crystalline structures: less perfect crystals (α′-form crystals), which have enough

time to melt and to reorganize into crystals with higher structural perfection (α-form crystals), before they remelt at higher temperature [34].

Table 3: Thermal properties of neat PLA and its composites

Samples	T_g (°C)	T_{cc} (°C)	T_m (°C)	ΔH_{cc} ($J \cdot g^{-1}$)	ΔH_m ($J \cdot g^{-1}$)	Xc (%)
PLA	63.3	133.5	165.9	5.9	9.5	3.9
MCC	–	–	–	–	–	–
PLA/20%MCC	62.5	109.3	169.1	16.3	20.5	5.5
PLA/5%-MCC-g-PCL	61.3	113.2	159.9	23.5	28.5	5.6
PLA/10%-MCC-g-PCL	61.3	108.0	168.8	23.3	34.6	13.4
PLA/15%-MCC-g-PCL	58.4	103.8	166.3	3.1	26.6	29.4
PLA/20%-MCC-g-PCL	60.7	110.6	167.4	13.4	25.9	16.6

Table 4: Mechanical properties of neat PLA and its composites

Samples	Tensile strength (MPa)	Elongation at break (%)	Young's modulus (MPa)	Impact strength (J/m)
PLA	65.1 ± 1.2	6 ± 1.4	1760 ± 70	20.6 ± 0.6
PLA/20%-MCC	56.7 ± 0.8	3.9 ± 1.0	1249 ± 51	18.1 ± 0.4
PLA/5%-MCC-g-PCL	61.4 ± 1.0	6.9 ± 0.9	826 ± 81	17.6 ± 0.5
PLA/10%-MCC-g-PCL	50.6 ± 0.7	11.5 ± 0.8	919 ± 84	22.5 ± 0.4
PLA/15%-MCC-g-PCL	47.3 ± 0.8	22.6 ± 0.7	760 ± 92	26.3 ± 0.5
PLA/20%-MCC-g-PCL	39.9 ± 0.9	30.5 ± 0.7	744 ± 67	17.9 ± 0.3

3.4 Mechanical Properties

The stress-strain curves of the samples are shown in Fig. 7. The tensile strength, elongation at break and impact strength of neat PLA and composites are also listed in Table 4. It is clearly observed from Table 4 that PLA/20%MCC composites have the lowest elongation at break and impact strength among all the samples due to phase separation induced by cellulose unite formation. The tensile strength of the PLA/MCC-g-PCL composites decreases with increasing the content of MCC-g-PCL. With addition of 20%MCC-g-PCL into PLA, the tensile strength of the composites is 39 MPa, which is 20% lower than that of PLA. However, the elongation at break of the PLA/MCC-g-PCL composites increases with increasing the content of MCC-g-PCL. The elongation at break of PLA/20%MCC-g-PCL has the highest value of 30.5%, which is increased by 400% compared to neat PLA. This is attributed to the MCC-g-PCL molecule as a polar molecule structure similar to that of the PLA molecular chain. Moreover, the successful grafting of PCL onto cellulose via ROP results in an expansion of intermolecular distance and an enhancement of the PLA chain mobility [28]. Simultaneously, the Young's modulus of PLA/MCC-g-PCL composites is lower than the neat PLA. With increasing the amount of MCC-g-PCL, the Young's modulus of the composites decrease monotonously, which was attributed to the CL segments in the MCC-g-PCL copolymer.

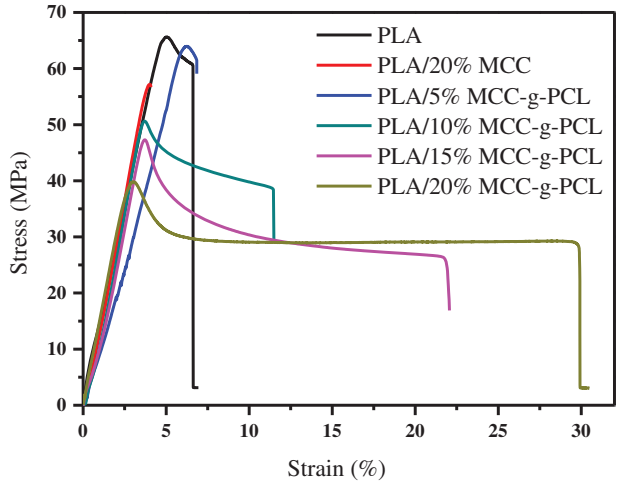

Figure 7: The stress-strain curves of neat PLA, binary blends, and PLA/MCC-g-PCL composites with different content of MCC-g-PCL

The impact strengths of PLA/MCC-g-PCL composites are also investigated. It is seen that the impact strength of the composites with 5%MCC-g-PCL is lower than that of neat PLA because a small amount of cellulose derivative cannot afford enough polar structure to combine with interface of PLA, thus a phase separation occurs between MCC-g-PCL and PLA. With increasing the content of MCC-g-PCL, the impact strengths of PLA/MCC-g-PCL composites increase because of more polar groups in the MCC-g-PCL. The interaction between MCC-g-PCL and hydrophobic surface PLA is strengthened. For 15% MCC-g-PCL composites, the impact strength reaches the maximum, 26 J/m, which is about 130% higher than that of neat PLA. However, when the MCC-g-PCL content increases to 20%, the impact strength of the composites decreases. This indicates that moderate MCC-g-PCL contents has a toughning effect on PLA/MCC-g-PCL composites, and the extra contents of MCC-g-PCL will generate some flaw. During the stretching process, the holes and wrinkles formed in the PLA phase as shown in SEM images play an important role in improving the impact strength of the composites.

3.5 Rheological Behavior

Chemorheology is a powerful way to study the flow and deformation of polymers from the viscoelastic response of the materials [32]. In order to study the rheological behavior of the samples, we record the variation of storage modulus (G′) (A), loss modulus (G″) (B) and complex viscosity (|η*|) (C) as a function of frequency for PLA and the composites (Fig. 8). Fig. 8A shows the storage modulus (G′) of all PLA/MCC-g-PCL samples exhibited a monotonous increase with sweeping frequency, which deviated obviously from terminal behavior at low sweeping frequency. It is found that the storage modulus (G′) and loss modulus (G″) decrease with increasing content of MCC-g-PCL, as shown in Figs. 8A and 8B, which is ascribing to MCC-g-PCL derivatives as a plasticizer increasing the free volume generated between polymer chains. The MCC-g-PCL derivative particles increase the distance between polymer molecular chains, weaken the entanglement between PLA molecular chains, and promote the movement ability of PLA molecular chains. The enhancement of deformation ability of the polymer chain results in the decrease of storage modulus during stretching. At the same time, the loss of deformation ability is reduced, which leads to a decrease in loss modulus.

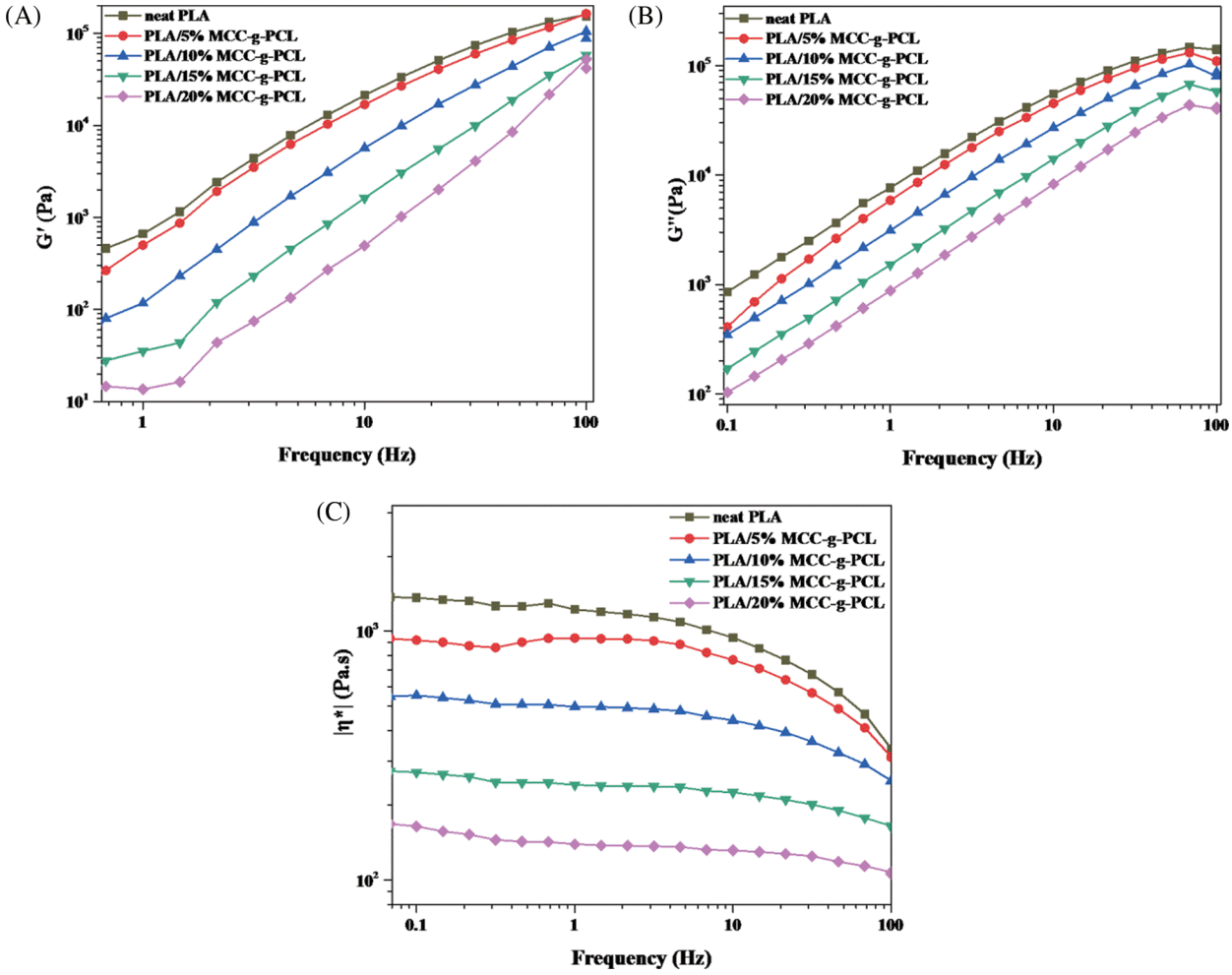

Figure 8: Variation of storage modulus (G′) (A), loss modulus (G″) (B) and complex viscosity (|η*|) (C) as a function of frequency for PLA and its composites

Except for storage modulus and loss modulus, the complex viscosity is also related to the microstructure of the sample, as shown in Fig. 8C. All samples showed shear thinning behavior, and the complex viscosity at a given frequency decreases rapidly with increasing in MCC-g-PCL content, which is attributed to the formation of greater free volume due to the enhancement of chain mobility. Meanwhile, higher crystallinity in PLA also lead to lower viscosity according to DSC results. Fig. 8C shows that pure PLA has a Newtonian platform at low frequency and a rapid decrease at high frequency range during the rheological test, exhibiting obvious linear viscoelasticity. MCC-g-PCL significantly reduces the complex viscosity of PLA due to the plasticization, however, shear thinning behavior are visibly weakened at high frequency. At low frequencies, the interaction between PLA molecular chains is not sensitive to external effects, and the entanglement between MCC-g-PCL particles and PLA molecular chains is deformed by external effects, showing a decrease in melt viscosity. The melt viscosity tends to be stable when the deformation between the particles and the PLA polymer chain tends to be stable at high frequency range.

3.6 Plastification Mechanism

The prepared plasticizer MCC-g-PCL is sustainable cellulose derivative with a flexible side chain of polyester structure, the good flexibility and processability of MCC-g-PCL depend on its structure. The PCL as a side chain was introduced into the MCC-g-PCL, which is easy to rotate freely owing to its C-C and C-O bond in the PCL molecular chain. The MCC-g-PCL with a flexible side chain unit allows PLA molecular chains conformational relaxation in plasticization process, leading to weak intermolecular interaction of PLA. Moreover, the PCL of MCC-g-PCL and PLA molecular chains segments are very similar, forming a interlaced state, and obtaining good compatibility in the composite matrix. In addition, the plasticizer MCC-g-PCL has a polar –COO– structure, which can significantly increase interaction force with PLA, thereby further weakening the interaction between the PLA molecules. As presented in the figure, the glass transition temperature of the PLA/MCC-g-PCL blends decreases, the elongation at break increases, and the complex viscosity decreases. On the other hand, the weak polar ester group of PCL is beneficial to the crystallization process in the condensed state. Increasing the introduction amount of MCC-g-PCL, the MCC-g-PCL molecules may be partially agglomerated, which is not conducive to the uniform distribution of the plasticizer in PLA. It is mainly attributed to the fact that only a small amount of plasticizer molecules interact with PLA molecules.

4 Conclusions

The MCC-g-PCL copolymer presents an interesting opportunity as a new sustainable plastic additive. In addition, both the MCC-g-PCL and PLA can meet the requirements of "double green" materials because they are all derived from natural resources. In summary, the results clearly demonstrate that MCC-g-PCL can be utilized to produce advanced green composites with the enhanced toughness without expensing the mechanical properties. When the addition of MCC-g-PCL is 15%, the PLA blends exhibited the highest impact strength, considerable elongation at break and moderate tensile strength. The rheological results showed that MCC-g-PCL as plasticizer, the introduction of PCL flexible chain increases the mobility of PLA molecular chain, and the complex viscosity, storage modulus and loss modulus of the blends decrease. DSC results showed that the addition of MCC-g-PCL reduced the T_g of the blend. When the addition amount was 15 wt%, the T_g of the blend was 58.4°C. MCC-g-PCL polyester plasticizer has better thermal stability, $T_{5\%}$ (°C) can still be maintained above 300°C. We therefore believe that this study provides a promising approach for manufacturing high-performance green materials by adding natural resources. Consequently, this study will provide a comprehensive understanding of the behaviors of the MCC-g-PCL during the processing of PLA modification and provide new opportunities for sustainable plasticizers. In particular, it provides prospects for application of cellulose-g-PCL derivatives as green plasticizers to modify bio-based polymers. To better understand the origin of such morphological and rheological observations, more detailed studies are certainly needed to complete these preliminary observations.

Funding Statement: This work was supported by the National Natural Science Foundation of China (21574030, 52063007, 51863004), Guizhou Province High-Level Innovative Talents Fund ([2020]6024), Guizhou Provincial Science and Technology Projects (Grant No. [2022]024) and the Science and Technology Project of Baiyun District, Guiyang City (Grant No. [2020]26), the authors gratefully acknowledge the financial support from the National Engineering Research Center for Compounding and Modification of Polymeric Materials (Guizhou Material Industrial Technology Institute).

Conflicts of Interest: The authors declare that they have no conflicts of interest to report regarding the present study.

References

1. Nasrollahzadeh, M., Sajjadi, M., Iravani, S., Varma, R. S. (2021). Starch, cellulose, pectin, gum, alginate, chitin and chitosan derived (nano) materials for sustainable water treatment: A review. *Carbohydrate Polymers, 251(48),* 116986. DOI 10.1016/j.carbpol.2020.116986.
2. Guillaume, S. M. (2022). Sustainable and degradable plastics. *Nature Chemistry, 14(3),* 245–246. DOI 10.1038/s41557-022-00901-8.
3. Baek, S., Lee, J., Kim, H., Cha, I., Song, C. (2021). Self-healable and recyclable biomass-derived polyurethane networks through carbon dioxide immobilization. *Polymers, 13(24),* 4381. DOI 10.3390/polym13244381.
4. Taib, N. A. A. B., Rahman, M. R., Huda, D., Kuok, K. K., Hamdan, S. et al. (2022). A review on poly lactic acid (PLA) as a biodegradable polymer. *Polymer Bulletin, 3(2)*. DOI 10.1007/s00289-022-04160-y.
5. Bass, G. F., Epps, T. H. (2021). Recent developments towards performance-enhancing lignin-based polymers. *Polymer Chemistry, 12(29),* 4130–4158. DOI 10.1039/D1PY00694K.
6. Souza, L. K. C., Martins, J. C., Oliveira, D. P., Ferreira, C. S., Araujo, R. O. et al. (2020). Hierarchical porous carbon derived from acai seed biowaste for supercapacitor electrode materials. *Journal of Materials Science-Materials in Electronics, 31(15),* 12148–12157. DOI 10.1007/s10854-020-03761-5.
7. Deng, F., Amarasekara, A. S. (2021). Catalytic upgrading of biomass derived furans. *Industrial Crops and Products, 159,* 113055. DOI 10.1016/j.indcrop.2020.113055.
8. Fortelny, I., Ujcic, A., Fambri, L., Slouf, M. (2019). Phase structure, compatibility, and toughness of PLA/PCL blends: A review. *Frontiers in Materials, 6,* 206. DOI 10.3389/fmats.2019.00206.
9. Sanivada, U. K., Marmol, G., Brito, F. P., Fangueiro, R. (2020). PLA composites reinforced with flax and jute fibers-a review of recent trends, processing parameters and mechanical properties. *Polymers, 12(10),* 2373. DOI 10.3390/polym12102373.
10. Milovanovic, S., Pajnik, J., Lukic, I. (2022). Tailoring of advanced poly(lactic acid)-based materials: A review. *Journal of Applied Polymer Science, 139(12),* 51839. DOI 10.1002/app.51839.
11. Song, X. Y., Wang, M., Weng, Y. X., Huang, Z. G. (2017). Effect of bamboo flour grafted lactide on the interfacial compatibility of polylactic acid/bamboo flour composites. *Polymers, 9(8),* 323. DOI 10.3390/polym9080323.
12. Kyutokua, H., Maeda, N., Sakamoto, H., Nishimuraa, H., Yamada, K. (2019). Effect of surface treatment of cellulose fiber (CF) on durability of PLA/CF bio-composites. *Carbohydrate Polymers, 203(1),* 95–102. DOI 10.1016/j.carbpol.2018.09.033.
13. Shamshina, J. L., Zavgorodnya, O., Berton, P., Chhotaray, P. K., Choudhary, H. et al. (2018). Ionic liquid platform for spinning composite chitin-poly (lactic acid) fibers. *ACS Sustainable Chemistry & Engineering, 6(8),* 10241–10251. DOI 10.1021/acssuschemeng.8b01554.
14. Zawada, K., Plichta, A., Janczewski, D., Hajmowicz, H., Florjanczyk, Z. et al. (2017). Esters of tartaric acid, a new class of potential double green plasticizers. *ACS Sustainable Chemistry & Engineering, 5(7),* 5999–6007. DOI 10.1021/acssuschemeng.7b00814.
15. Si, W. J., Yuan, W. Q., Li, Y. D., Chen, Y. K., Zeng, J. B. (2018). Tailoring toughness of fully biobased poly(lactic acid)/natural rubber blends through dynamic vulcanization. *Polymer Testing, 65,* 249–255. DOI 10.1016/j.polymertesting.2017.11.030.
16. Bocque, M., Voirin, C., Lapinte, V., Caillol, S., Robin, J. J. (2016). Petro-based and bio-based plasticizers: Chemical structures to plasticizing properties. *Journal of Polymer Science Part A: Polymer Chemistry, 54(1),* 11–33. DOI 10.1002/pola.27917.
17. Zhao, T. H., Yuan, W. Q., Li, Y. D., Weng, Y. X., Zeng, J. B. (2018). Relating chemical structure to toughness via morphology control in fully sustainable sebacic acid cured epoxidized soybean oil toughened polylactide blends. *Macromolecules, 51(5),* 2027–2037. DOI 10.1021/acs.macromol.8b00103.
18. Vacaras, S., Baciut, M., Lucaciu, O., Dinu, C., Baciut, G. et al. (2019). Understanding the basis of medical use of poly-lactide-based resorbable polymers and composites–A review of the clinical and metabolic impact. *Drug Metabolism Reviews, 51(4),* 570–588. DOI 10.1080/03602532.2019.1642911.
19. Mohanty, A. K., Vivekanandhan, S., Pin, J. M., Misra, M. (2018). Composites from renewable and sustainable resources: Challenges and innovations. *Science, 362(6414),* 536–542. DOI 10.1126/science.aat9072.

20. Zhang, J., Qi, Y., Shen, Y., Li, H. (2022). Research progress on chemical modification and application of cellulose: A review. *Materials Science-Medziagotyra, 28(1),* 60–67. DOI 10.5755/j02.ms.25485.
21. Rose, M., Palkovits, R. (2011). Cellulose-based sustainable polymers: State of the art and future trends. *Macromolecular Rapid Communications, 32(17),* 1299–1311. DOI 10.1002/marc.201100230.
22. Ghiat, I., Al-Ansari, T. (2021). A review of carbon capture and utilisation as a CO_2 abatement opportunity within the EWF nexus. *Journal of CO_2 Utilization, 45,* 101432. DOI 10.1016/j.jcou.2020.101432.
23. Gleizer, S., Bar-On, Y. M., Ben-Nissan, R., Milo, R. (2020). Engineering microbes to produce fuel, commodities, and food from CO_2. *Cell Reports Physical Science, 1(10),* 100223. DOI 10.1016/j.xcrp.2020.100223.
24. Xie, H. B., Yu, X., Yang, Y., Zhao, Z. K. (2014). Capturing CO_2 for cellulose dissolution. *Green Chemistry, 16(5),* 2422–2427. DOI 10.1039/c3gc42395f.
25. Zhang, Q., Oztekin, N. S., Barrault, J., De Oliveira Vigier, K., Jérôme, F. (2013). Activation of microcrystalline cellulose in a CO_2-based switchable system. *ChemSusChem, 6(4),* 593–596. DOI 10.1002/cssc.201200815.
26. Dai, L., Xiao, S., Shen, Y., Qinshu, B., He, J. (2012). The synthesis of cellulose-graft-poly (L-lactide) by ring-opening polymerization and the study of its degradability. *Bulletin of the Korean Chemical Society, 33(12),* 4122–4126. DOI 10.5012/bkcs.2012.33.12.4122.
27. Lönnberg, H., Zhou, Q., Brumer, H., Teeri, T. T., Malmström, E. et al. (2006). Grafting of cellulose fibers with poly (ε-caprolactone) and poly (l-lactic acid) via ring-opening polymerization. *Biomacromolecules, 7(7),* 2178–2185. DOI 10.1021/bm060178z.
28. Xu, Q., Song, L., Zhang, L., Hu, G., Du, J. et al. (2017). Organocatalytic cellulose dissolution and in situ grafting of ε-caprolactone via ROP in a reversible DBU/DMSO/CO_2 system. *ChemistrySelect, 2(24),* 7128–7134. DOI 10.1002/slct.201701639.
29. Vidéki, B., Klébert, S., Pukánszky, B. (2005). Grafting of caprolacton to cellulose acetate by reactive processing. *European Polymer Journal, 41(8),* 1699–1707. DOI 10.1016/j.eurpolymj.2005.03.002.
30. Sheng, K., Zhang, S., Qian, S., Lopez, C. A. F. (2019). High-toughness PLA/Bamboo cellulose nanowhiskers bionanocomposite strengthened with silylated ultrafine bamboo-char. *Composites Part B: Engineering, 165,* 174–182. DOI 10.1016/j.compositesb.2018.11.139.
31. Xu, L., Zhao, J., Qian, S., Zhu, X., Takahashi, J. (2021). Green-plasticized poly (lactic acid)/nanofibrillated cellulose biocomposites with high strength, good toughness and excellent heat resistance. *Composites Science and Technology, 203(13),* 108613. DOI 10.1016/j.compscitech.2020.108613.
32. Hiltunen, K., Seppälä, J. V., Härkönen, M. (1997). Effect of catalyst and polymerization conditions on the preparation of low molecular weight lactic acid polymers. *Macromolecules, 30(3),* 373–379. DOI 10.1021/ma960919w.
33. Chen, Y., Yuan, D., Xu, C. (2014). Dynamically vulcanized biobased polylactide/natural rubber blend material with continuous cross-linked rubber phase. *ACS Applied Materials & Interfaces, 6(6),* 3811–3816. DOI 10.1021/am5004766.
34. Zhao, T. H., Wu, Y., Li, Y. D., Wang, M., Zeng, J. B. (2017). High performance and thermal processable dicarboxylic acid cured epoxidized plant oil resins through dynamic vulcanization with poly (lactic acid). *ACS Sustainable Chemistry & Engineering, 5(2),* 1938–1947. DOI 10.1021/acssuschemeng.6b02684.